Resetting proteostasis with ISRIB promotes epithelial differentiation to attenuate pulmonary fibrosis

Satoshi Watanabe[a,b], Nikolay S. Markov[a], Ziyan Lu[a], Raul Piseaux Aillon[a], Saul Soberanes[a], Constance E. Runyan[a], Ziyou Ren[a], Rogan A. Grant[a], Mariana Maciel[a], Hiam Abdala-Valencia[a], Yuliya Politanska[a], Kiwon Nam[a], Lango Sichizya[a], Hermon G. Kihshen[a], Nikita Joshi[a], Alexandra C. McQuattie-Pimentel[a], Katherine A. Gruner[c], Manu Jain[a], Jacob I. Sznajder[a], Richard I. Morimoto[d], Paul A. Reyfman[a], Cara J. Gottardi[a], G. R. Scott Budinger[a,1,2], and Alexander V. Misharin[a,1,2]

[a]Department of Medicine, Division of Pulmonary and Critical Care Medicine, Feinberg School of Medicine, Northwestern University, Chicago, IL 60611; [b]Department of Respiratory Medicine, Kanazawa University Graduate School of Medical Sciences, Kanazawa 920-8641, Japan; [c]Mouse Histology and Phenotyping Laboratory, Robert H. Lurie Comprehensive Cancer Center, Northwestern University, Chicago, IL 60611; and [d]Department of Molecular Biosciences, Northwestern University, Evanston, IL 60208

Edited by Christopher K. Glass, University of California San Diego, La Jolla, CA, and approved March 26, 2021 (received for review January 20, 2021)

Pulmonary fibrosis is a relentlessly progressive and often fatal disease with a paucity of available therapies. Genetic evidence implicates disordered epithelial repair, which is normally achieved by the differentiation of small cuboidal alveolar type 2 (AT2) cells into large, flattened alveolar type 1 (AT1) cells as an initiating event in pulmonary fibrosis pathogenesis. Using models of pulmonary fibrosis in young adult and old mice and a model of adult alveologenesis after pneumonectomy, we show that administration of ISRIB, a small molecule that restores protein translation by EIF2B during activation of the integrated stress response (ISR), accelerated the differentiation of AT2 into AT1 cells. Accelerated epithelial repair reduced the recruitment of profibrotic monocyte-derived alveolar macrophages and ameliorated lung fibrosis. These findings suggest a dysfunctional role for the ISR in regeneration of the alveolar epithelium after injury with implications for therapy.

proteostasis | fibrosis | ISRIB

Pulmonary fibrosis is a relentlessly progressive and often fatal disease characterized by the replacement of normal lung tissue with fibrotic scar that increases the work of breathing and impairs gas exchange (1, 2). Advanced age is among the most important risk factors for the development of pulmonary fibrosis (3), and even in patients with a genetic predisposition, the onset of disease seldom occurs before the sixth decade, and the incidence increases exponentially with advancing age (4, 5). The development of cellular senescence, mitochondrial dysfunction, stem cell exhaustion, and proteostatic stress have all been implicated in the age-related susceptibility to pulmonary fibrosis, but our understanding of the underlying molecular mechanisms is incomplete (6, 7).

Proteostasis refers to the dynamic process by which cells control the concentration, conformation, binding interactions, and stability of individual proteins making up the proteome via regulated networks that influence protein synthesis, folding, trafficking, disaggregation, and degradation (8, 9). Analyses of families with high rates of pulmonary fibrosis as well as unbiased genetic studies in populations of patients with idiopathic pulmonary fibrosis (IPF) identified associations between mutations in genes predicted to disrupt proteostasis in the alveolar epithelium and the development of pulmonary fibrosis (10). Furthermore, an extensive body of literature in aging animals and humans implicates a decline in proteostasis resilience with advancing age (11, 12). Proteostatic stress activates the family of eukaryotic translation initiation factor 2 alpha kinases 1 to 4 (EIF2AK1, also known as HRI; EIF2AK2, also known as PKR; EIF2AK3, also known as PERK; and EIF2AK4, also known as GCN2), triggering the integrated stress response (ISR) (13). Activation of the ISR reduces the rate of global protein translation while enhancing the translation of selected transcription factors, including ATF4, that induce the expression of chaperones and other cell-protective genes. Prolonged or high-level induction of the ATF4 target gene *DDIT3*, also known as C/EBP homologous protein (CHOP), activates apoptotic pathways that result in cell death (14). Notably, the ISR is activated via EIF2AK2 in response to viral infections, which have been implicated in exacerbations of IPF (15). Previous studies in animal models have suggested that activation of the ISR contributes to the development of pulmonary fibrosis, but the mechanisms are incompletely understood (16–19).

We suggest a multicellular model of pulmonary fibrosis pathogenesis that explains many observations in patients and animal models. Fibrosis begins when an environmental insult, for example, a viral infection or toxic dust like asbestos, injures the alveolar epithelium. The resulting injury leads to the recruitment of monocyte-derived alveolar macrophages to the alveolar space where they come into direct contact with fibroblasts in the matrix (20–31). Monocyte-derived alveolar macrophages express *CSF1R*, which encodes M-CSF-R, and fibroblasts secrete M-CSF (encoded by *CSF1*), creating a signaling loop that retains monocyte-derived alveolar

Significance

Disordered epithelial proteostasis is strongly implicated in the pathobiology of pulmonary fibrosis. We found that a small molecule that specifically restores protein translation by EIF2B during activation of the integrated stress response, ISRIB, attenuated the severity of pulmonary fibrosis in young adult and old mice. Our data support a multicellular model of fibrosis in which relieving a block to epithelial differentiation induced by activation of the integrated stress response slows the recruitment of profibrotic monocyte-derived alveolar macrophages to attenuate pulmonary fibrosis. A loss of proteostasis resilience in aging would further slow repair, perhaps explaining the increased risk of fibrosis in the elderly.

Author contributions: S.W., H.A.-V., M.J., J.I.S., R.I.M., C.J.G., G.R.S.B., and A.V.M. designed research; S.W., N.S.M., Z.L., R.P.A., S.S., C.E.R., Z.R., R.A.G., M.M., H.A.-V., Y.P., K.N., L.S., H.G.K., N.J., A.C.M.-P., K.A.G., and P.A.R. performed research; S.W., N.S.M., Z.L., S.S., C.E.R., Z.R., R.A.G., M.M., H.A.-V., K.A.G., M.J., J.I.S., R.I.M., C.J.G., G.R.S.B., and A.V.M. analyzed data; and S.W., N.S.M., R.A.G., M.J., J.I.S., R.I.M., C.J.G., G.R.S.B., and A.V.M. wrote the paper.

The authors declare no competing interest.

This article is a PNAS Direct Submission.

[1]G.R.S.B. and A.V.M. contributed equally to this work.

[2]To whom correspondence may be addressed. Email: s-buding@northwestern.edu or a-misharin@northwestern.edu.

This article contains supporting information online at https://www.pnas.org/lookup/suppl/doi:10.1073/pnas.2101100118/-/DCSupplemental.

Published May 10, 2021.

macrophages in the niche (24). In turn, monocyte-derived alveolar macrophages secrete molecules that promote fibroblast differentiation and proliferation, driving the development of fibrosis (32, 33). The regenerating epithelium disrupts interactions between monocyte-derived alveolar macrophages and fibroblasts while simultaneously providing signals (e.g., GM-CSF) to monocyte-derived alveolar macrophages that promote their differentiation into homeostatic cells resembling tissue-resident alveolar macrophages or to undergo apoptosis. In the presence of a challenge to proteostasis induced by genetic abnormalities, advanced age, or both, this process is impaired, the epithelial barrier is not restored, and the macrophage/fibroblast circuits persist. Eventually, proliferating fibroblasts lose their dependence on signals from alveolar macrophages, resulting in fibroblast expansion and matrix deposition characteristic of end stage pulmonary fibrosis (32, 33).

This model predicts that strategies to improve proteostasis in the alveolar epithelium should promote the proliferation of alveolar type 2 (AT2) cells or promote their differentiation into alveolar type 1 (AT1) cells, accelerated by the differentiation of profibrotic monocyte-derived alveolar macrophages and ameliorate fibrosis. Carmela Sidrauski and colleagues (34) in Peter Walter's laboratory identified a small molecule inhibitor of the integrated stress response, ISRIB. ISRIB enhances the guanine exchange factor activity of the eukaryotic initiation factor 2B (eIF2B), relieving both the translational inhibition induced by activation of the ISR and preventing gene expression induced by ATF4 (34, 35). ISRIB has shown promise as a therapeutic strategy against inflammation, cancer, and neurocognitive diseases in aging (34, 36). We found that ISRIB ameliorated fibrosis in both young adult and old mice. The administration of ISRIB accelerated the differentiation of AT2 into AT1 cells and reduced the recruitment of profibrotic monocyte-derived alveolar macrophages. Consistently, a single dose of ISRIB enhanced the differentiation of AT2 into AT1 cells after pneumonectomy in young adult mice. Our results suggest activation of the ISR forms a proteostatic barrier to alveolar epithelial differentiation that is reduced by ISRIB.

Results

Old Mice Develop More Severe Lung Fibrosis in Response to Intratracheal Bleomycin and Asbestos. We induced lung fibrosis in young adult mice (3 to 5 mo) and old mice (18 to 24 mo) via the intratracheal administration of bleomycin (0.025 unit/50 μL) and analyzed the lungs 28 d later (Fig. 1 *A*–*D*). Old mice developed more severe lung fibrosis compared with young adult mice as evidenced by decreased lung compliance, elevated collagen levels, and worsened lung pathology (Fig. 1 *A* and *B*). While collagen levels in young mice returned to the near-normal levels, increased collagen levels persisted in old mice for up to 56 d (Fig. 1*C*). Both young adult and old mice lost body weight after the instillation of bleomycin. However, while body weight recovered in young adult mice, it failed to recover in old animals (Fig. 1*D*).

We observed a similar age-related susceptibility in a nonresolving model of pulmonary fibrosis induced by the intratracheal administration of crocidolite asbestos (100 μg/50 μL) (24, 37). In young adult mice exposed to intratracheal asbestos, we observed mild peribronchial fibrosis as evidenced by histological scoring of Masson's trichrome-stained lung sections, but body weight and lung compliance were not changed (Fig. 1 *E*–*H*). In contrast, old animals lost and did not recover body weight and had reduced lung compliance, increased lung collagen levels, and increased fibrosis 28 d after asbestos administration (Fig. 1 *E*–*H*). Collagen levels remained increased up to 56 d after asbestos administration (Fig. 1*G*). Thus, advanced age is associated with worsened and prolonged fibrosis in both bleomycin- and asbestos-induced models of pulmonary fibrosis.

Recruitment of Pathogenic Monocyte-Derived Alveolar Macrophages Is Increased during Lung Fibrosis in Old Mice. We and others have performed causal genetic studies in mice to show that monocyte-derived alveolar macrophages are necessary for the development of bleomycin- and asbestos-induced lung fibrosis independent of circulating monocytes, tissue-resident interstitial macrophages, or tissue-resident alveolar macrophages (20–24). Nureki et al. causally linked disordered epithelial proteostasis with the recruitment of these profibrotic monocyte-derived alveolar macrophages by showing lung epithelial–specific expression of a mutant form of the surfactant protein C gene associated with pulmonary fibrosis in children was sufficient to drive their recruitment (27). Therefore, we asked whether the increased severity of lung fibrosis in old mice is associated with an increased recruitment of monocyte-derived alveolar macrophages. We quantified myeloid cell populations in the lung via flow cytometry 28 d after the administration of bleomycin or asbestos as previously described (22) (Fig. 2 and *SI Appendix*, Fig. S1). We used differential expression of Siglec F to separate monocyte-derived alveolar macrophages ($CD64^+$Siglec F^{low}) from tissue-resident alveolar macrophages ($CD64^+$Siglec F^{high}) (22, 38). We found that classical monocytes, T cells, and B cells were increased in the lungs of old mice both in the steady state and during asbestos-induced fibrosis as has been reported (Fig. 2 and *SI Appendix*, Fig. S2) (39). After the intratracheal instillation of either bleomycin or asbestos, interstitial macrophages ($CD64^+$Siglec F^-) and monocyte-derived alveolar macrophages were increased in old compared to young adult mice (Fig. 2 *A* and *B*).

ISRIB Ameliorates Lung Fibrosis in Young and Old Mice. We treated young adult and old mice with a small molecule inhibitor of the integrated stress response, ISRIB (2.5 mg/kg via intraperitoneal injections) or vehicle, daily starting at day 7 after instillation of bleomycin and continued until harvest at day 28 (Fig. 3*A*). In both young adult and old mice, treatment with ISRIB resulted in higher lung compliance, lower collagen levels, and reduced histologic evidence of fibrosis as measured by blinded scoring of randomly selected lung sections stained with Masson's trichrome and attenuated weight loss when compared to vehicle-treated mice (Fig. 3 *B*–*G*). The administration of ISRIB in naïve old or young adult mice did not affect body weight, lung compliance, collagen levels, or induce detectable histologic changes.

We next tested the therapeutic efficacy of ISRIB in nonresolving fibrosis induced by intratracheal asbestos. Young adult and old mice were treated with crocidolite asbestos (100 μg/50 μL) and then treated with ISRIB (2.5 mg/kg via intraperitoneal injections) or vehicle daily beginning 7 d postinstillation. The lungs were harvested and analyzed 28 d after asbestos treatment (*SI Appendix*, Fig. S3*A*). In both young adult and old mice, treatment with ISRIB was associated with reduced fibrosis as measured by blinded scoring of Masson's trichrome-stained lung sections (*SI Appendix*, Fig. S3 *B*–*F*). As the dynamic range of collagen levels using picrosirius red precipitation after asbestos exposure is limited, we utilized second harmonic generation microscopy for quantitative analysis of collagen (40). Both young adult and old mice treated with ISRIB showed a decrease in lung collagen compared to vehicle-treated mice (*SI Appendix*, Fig. S3 *C* and *F*). In addition, young adult mice treated with ISRIB recovered body weight faster than vehicle-treated mice (*SI Appendix*, Fig. S3 *D* and *G*). Together, these data suggest that ISRIB ameliorates lung fibrosis in both young adult and old mice in both resolving and nonresolving models of pulmonary fibrosis.

Previous studies have demonstrated that even a single dose of ISRIB could dramatically ameliorate ISR-driven diseases (34, 36, 41). Accordingly, we treated mice with a single dose of ISRIB or vehicle before or 7 d after administration of bleomycin and assessed fibrosis severity 21 d later (*SI Appendix*, Fig. S4). Mice treated with a single dose of ISRIB showed reduced histologic

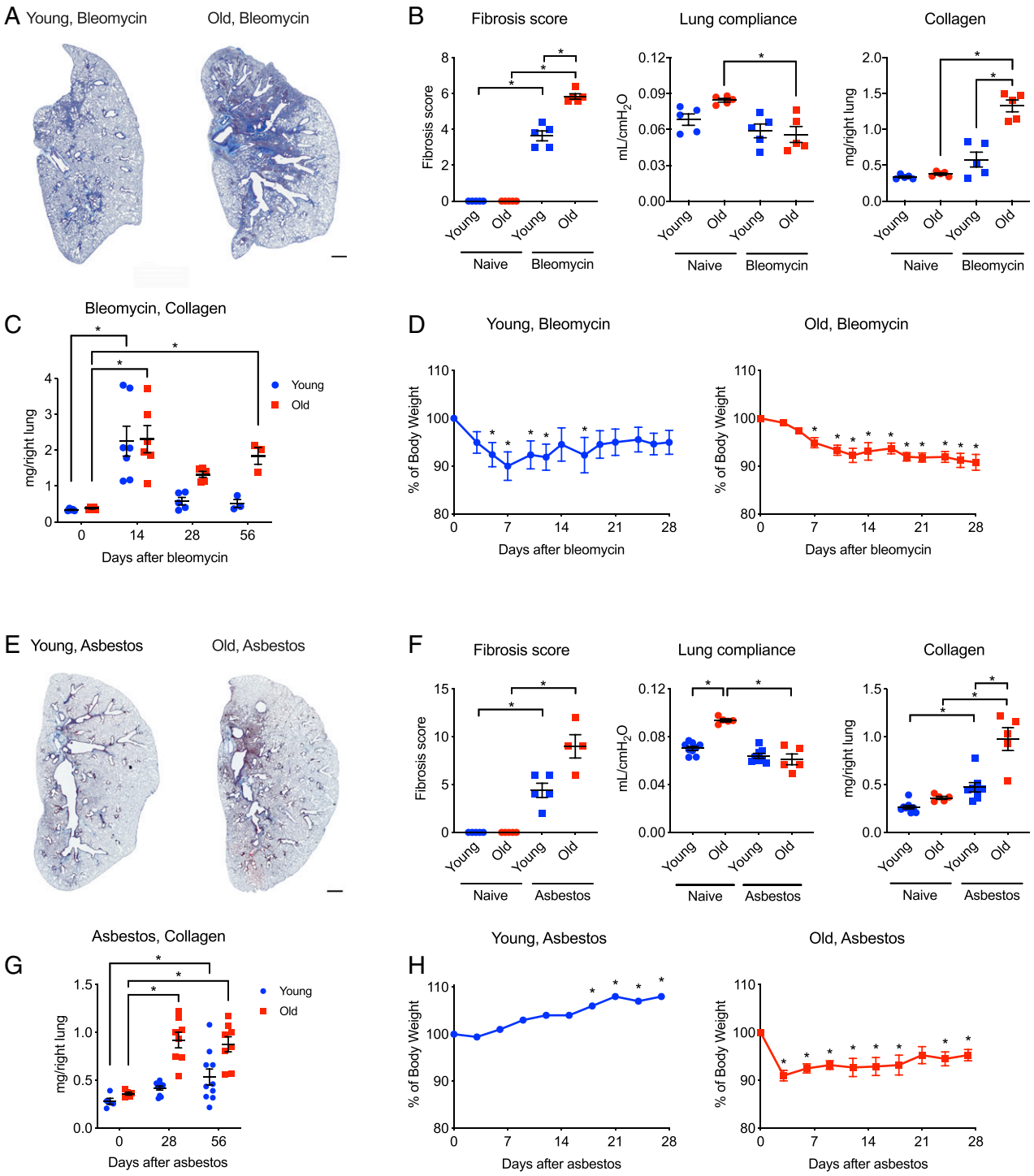

Fig. 1. Old mice develop more severe lung fibrosis compared to young adult mice. Young adult mice (3 to 5 mo) and old mice (18 to 24 mo) were administered bleomycin (0.025 unit/50 μL) or crocidolite asbestos (100 μg/50 μL) intratracheally, and the lungs were harvested as indicated. (*A*) Representative histologic images 28 d after bleomycin (Masson's trichrome). (Scale bar, 1 mm.) (*B*) Ashcroft fibrosis score (Mann–Whitney *U* test with Bonferroni correction for multiple comparisons), lung compliance using Flexivent (one-way ANOVA with Tukey test for multiple comparisons), and soluble collagen in lung homogenates 28 d after bleomycin (one-way ANOVA with Tukey test for multiple comparisons). (*C*) Soluble collagen 0, 14, 28, and 56 d after the administration of bleomycin. Two-way ANOVA with Dunnett's multiple comparisons test, comparing data from each day to baseline (day 0). (*D*) Body weight in young adult and old mice after the administration of bleomycin. Kruskal–Wallis test with Dunn's multiple comparisons test, comparing data from each day to baseline (day 0). (*E*) Representative histologic images 28 d after the administration of asbestos (Masson's trichrome). (Scale bar, 1 mm.) (*F*) Ashcroft fibrosis score (Mann–Whitney *U* tests with Bonferroni correction for multiple comparisons), lung compliance using Flexivent (one-way ANOVA with Tukey test for multiple comparisons), and soluble collagen in lung homogenates 28 d after the administration of asbestos (one-way ANOVA with Tukey test for multiple comparisons). (*G*) Soluble collagen 0, 28, and 56 d after the administration of asbestos. Two-way ANOVA with Dunnett's multiple comparisons test, comparing data from each day to baseline (day 0). (*H*) Body weight in young adult and old mice after the administration of asbestos. Kruskal–Wallis test with Dunn's multiple comparisons test, comparing data from each day to baseline (day 0). All data presented as mean ± SEM, 5 to 10 mice per group. $*P < 0.05$. Representative data from one of two independent experiments.

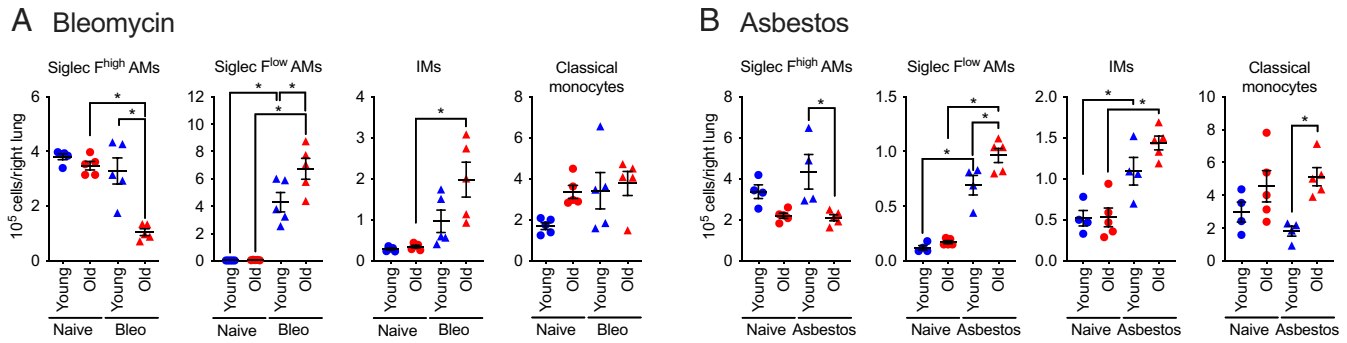

Fig. 2. Lung fibrosis is associated with an increased number of monocyte-derived alveolar macrophages in old mice. Young adult mice (3 to 5 mo) and old mice (18 to 24 mo) were administered bleomycin (0.025 unit/50 μL, intratracheally) or crocidolite asbestos (100 μg/50 μL, intratracheally), and the lungs were harvested 28 d later. Monocyte and macrophage populations in (*A*) bleomycin-induced lung fibrosis (Bleo) and (*B*) asbestos-induced lung fibrosis were quantified via flow cytometry. Data presented as mean ± SEM, number of mice shown on the plot, one-way ANOVA with Tukey test for multiple comparisons. $*P < 0.05$. Representative data from two independent experiments.

evidence of fibrosis as measured by blinded scoring of randomly selected lung sections stained with Masson's trichrome, improved lung compliance, and decreased collagen levels whether ISRIB was given with, or 7 d after, bleomycin (*SI Appendix*, Fig. S4).

ISRIB Reduces the Recruitment of Profibrotic Monocyte-Derived Alveolar Macrophages to the Lung. We treated mice with bleomycin and 7 d later started treatment with ISRIB (2.5 mg/kg, daily via intraperitoneal injections) followed by analysis of myeloid and lymphoid cells in the lung via flow cytometry at day 21. In young adult mice, the administration of ISRIB did not change the number of tissue-resident alveolar macrophages ($CD64^+$Siglec F^{high}) but reduced the number of monocyte-derived alveolar macrophages ($CD64^+$Siglec F^{low}), interstitial macrophages ($CD64^+$Siglec F^-), and lung classical monocytes (Fig. 4*A*). Similar changes were observed in old mice, except the number of lung classical monocytes was not affected by ISRIB (Fig. 4*B*).

We used a tamoxifen-inducible genetic lineage tracing system ($Cx3cr1^{ERCre} \times zsGreen^{LSL}$ mice) to measure the recruitment and fate of monocyte-derived alveolar macrophages after bleomycin. Classical monocytes, which are precursors for monocyte-derived alveolar macrophages, have a half-life of ~5 to 7 d in mice (*SI Appendix*, Fig. S5 *A* and *B*) (42). Therefore, only monocyte-derived alveolar macrophages recruited within this window of time after tamoxifen administration will be permanently labeled with GFP. First, we administered tamoxifen simultaneously with bleomycin to $Cx3cr1^{ERCre} \times zsGreen^{LSL}$ mice and started treatment with ISRIB at day 7, harvesting lungs for analysis on days 14, 28, and 56 (Fig. 5*A* and *SI Appendix*, Fig. S5*A*). We found that in bleomycin-induced fibrosis, the number of GFP^+Siglec F^{low} monocyte-derived alveolar macrophages recruited during the first 14 d remained stable over time (Fig. 5 *B* and *C*). This suggests that monocyte-derived alveolar macrophages are recruited as a single wave in the first 14 d after bleomycin administration and persist during the development of fibrosis. Administration of tamoxifen at day 21 or day 49 confirmed a lack of ongoing recruitment during the later stages (Fig. 5*D*). In asbestos-induced lung fibrosis, where epithelial injury persists over time, we found that monocyte-derived alveolar macrophages recruited early during the course of lung fibrosis persisted over time (*SI Appendix*, Fig. S5 *C–E*). In contrast to bleomycin, the administration of tamoxifen at later time points (days 14, 35, and 56) demonstrated ongoing recruitment of monocyte-derived alveolar macrophages during asbestos-induced lung fibrosis (*SI Appendix*, Fig. S5*F*). Old mice had fewer Siglec F^{high} tissue-resident alveolar macrophages at all time points compared to young adult mice. However, the kinetics of recruitment of monocyte-derived alveolar macrophages were similar in young adult and old mice (*SI Appendix*, Fig. S5*G*).

Treatment with ISRIB decreased the number of GFP^+Siglec F^{low} monocyte-derived alveolar macrophages at day 14 after bleomycin in both young adult and old mice (Fig. 5 *E* and *F*). To determine whether this reduction of monocyte-derived alveolar macrophages after treatment with ISRIB was attributable to reduced proliferation, we treated mice with EdU for 3 d before harvest. We found that after administration of bleomycin, tissue-resident and monocyte-derived alveolar macrophages in old mice showed increased incorporation of EdU compared with young adult mice (*SI Appendix*, Fig. S5 *H–J*). The enhanced proliferation of tissue-resident and monocyte-derived alveolar macrophages in old mice 21 d after bleomycin was not observed in ISRIB-treated mice. Collectively, these results suggest that ISRIB either reduces the recruitment or inhibits factors required for the maintenance of monocyte-derived alveolar macrophages during bleomycin-induced fibrosis irrespective of age.

Transcriptomic Profiling of Alveolar Macrophages and AT2 Cells Suggests ISRIB Targets AT2 Cells to Accelerate the Maturation of Monocyte-Derived Alveolar Macrophages. The transcription factor ATF4 activates a gene program that induces the expression of genes that remediate stress damage or induce apoptosis via CHOP (*DDIT3*/*Ddit3*). Under nonstressed conditions, ATF4 translation is prevented by ribosome binding to an inhibitory upstream open reading frame (uORF) that inhibits translation. The inhibition of global translation induced by activation of the ISR allows ribosomal binding to this uORF, allowing ATF4 translation to proceed (43). Because ISRIB removes the translational inhibition induced by activation of the ISR, it is predicted to reduce the expression of ATF4 target genes. Hence, we used RNA sequencing (RNA-seq) to ask the following: 1) In which cells are ATF4 target genes increased during fibrosis in young or old mice? 2) Do we see changes in the expression of those genes with ISRIB? Since we found that ISRIB decreased recruitment of the monocyte-derived alveolar macrophages, we evaluated transcriptomic changes in their precursors, classical monocytes, flow sorted from the lungs of young adult and old naïve mice treated with ISRIB for 7 d. Principal component analysis demonstrated a lack of variance in the data related to either aging or treatment with ISRIB (*SI Appendix*, Fig. S6*A*). A direct pairwise comparison between the groups identified only two differentially expressed genes (false discovery rate [FDR] $q < 0.05$ in ANOVA-like test) between ISRIB- and vehicle-treated mice irrespective of age (Dataset S1), suggesting that treatment with ISRIB does not substantially modify monocyte transcriptomic identity.

Next, we examined flow-sorted monocyte-derived alveolar macrophages 21 d after induction of bleomycin-induced lung fibrosis in young and old mice with or without treatment with ISRIB (Fig. 6*A*

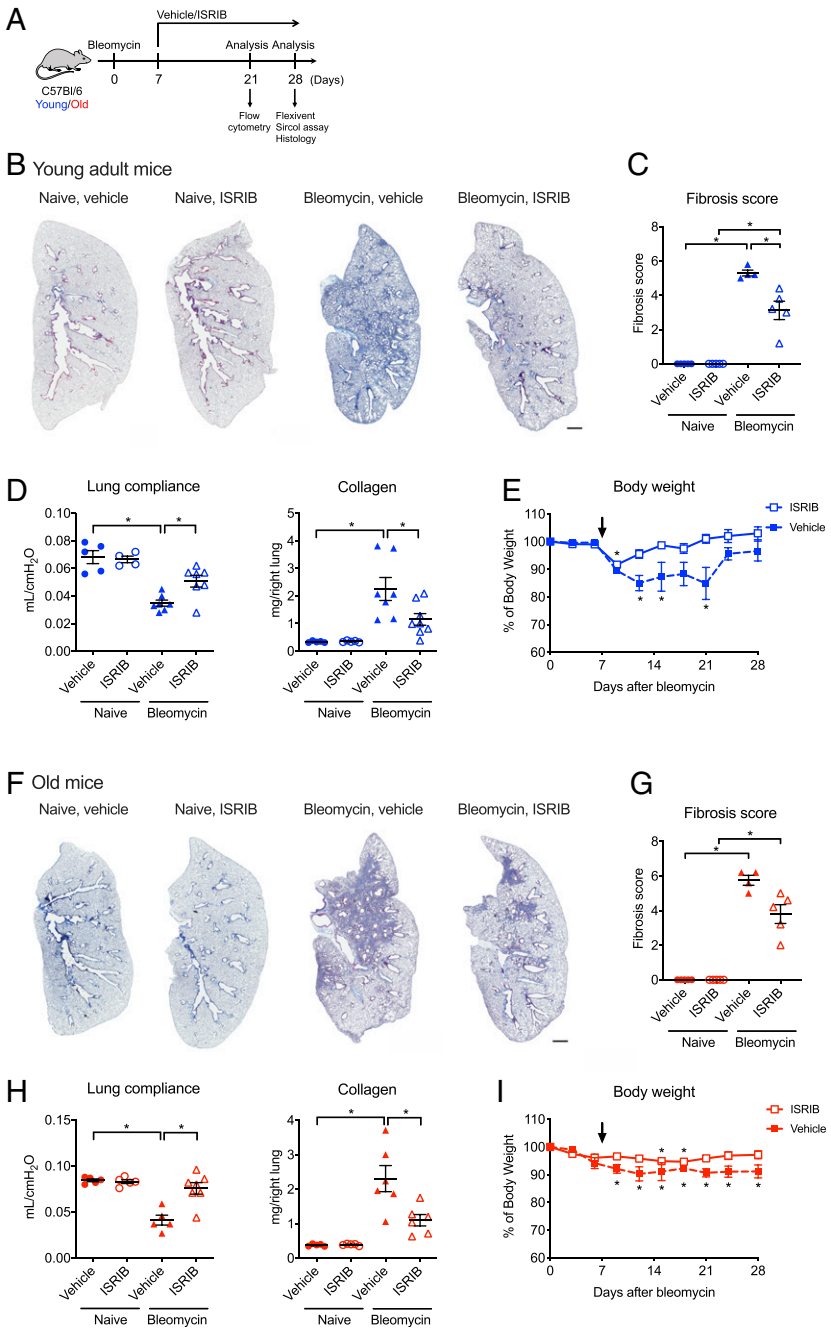

Fig. 3. Therapy with ISRIB attenuates bleomycin-induced lung fibrosis in young adult and old mice. (*A*) Schematic of the experimental design. Young adult (3 to 5 mo) and old (18 to 24 mo) mice were administered bleomycin (0.025 unit/50 μL, intratracheally) and treated with 2.5 mg/kg of ISRIB or vehicle (intraperitoneally daily) beginning at day 7 and harvested at the indicated time points. (*B*) Representative images of lung tissue from young adult naïve or bleomycin-treated mice, with or without ISRIB on day 28. Masson's trichrome staining. (Scale bar, 1 mm.) (*C*) Ashcroft fibrosis score (Mann–Whitney *U* tests with Bonferroni multiple test correction). (*D*) Lung compliance and collagen levels from young adult naïve or bleomycin-treated mice, with or without ISRIB (one-way ANOVA with Tukey test for multiple comparisons). (*E*) Body weight of young adult mice after administration of bleomycin, with or without ISRIB treatment, five mice per each group. The arrow indicates the start of ISRIB treatment (one-way ANOVA with Dunnet's multiple comparisons test). (*F*) Representative images of lung tissue from old naïve or bleomycin-treated mice, with or without ISRIB on day 28. Masson's trichrome staining. (Scale bar, 1 mm.) (*G*) Ashcroft fibrosis score (Mann–Whitney *U* tests with Bonferroni multiple test correction). (*H*) Lung compliance and collagen levels from old naïve mice or bleomycin-treated mice, with or without ISRIB (one-way ANOVA with Tukey test for multiple comparisons). (*I*) Body weight of old mice after administration of bleomycin, with or without ISRIB treatment, five mice per each group. The arrow indicates the start of ISRIB treatment (one-way ANOVA with Dunnet's multiple comparisons test). Data are shown as mean ± SEM, 5 to 7 mice per group. $*P < 0.05$. Representative data from two independent experiments.

and *SI Appendix*, Fig. S6*B*). Principal component analysis demonstrated that treatment with ISRIB and age were the main sources of variance in the dataset (PC1 29.7% and PC2 12.2%, respectively) (*SI Appendix*, Fig. S6*B*). *k*-means clustering on 1,923 differentially expressed genes (ANOVA-like test, FDR *q*-value < 0.05) identified five clusters reflecting age and ISRIB treatment status (Fig. 6*A* and Datasets S2 and S3). We did not identify enrichment for a curated list of ATF4 target genes in any

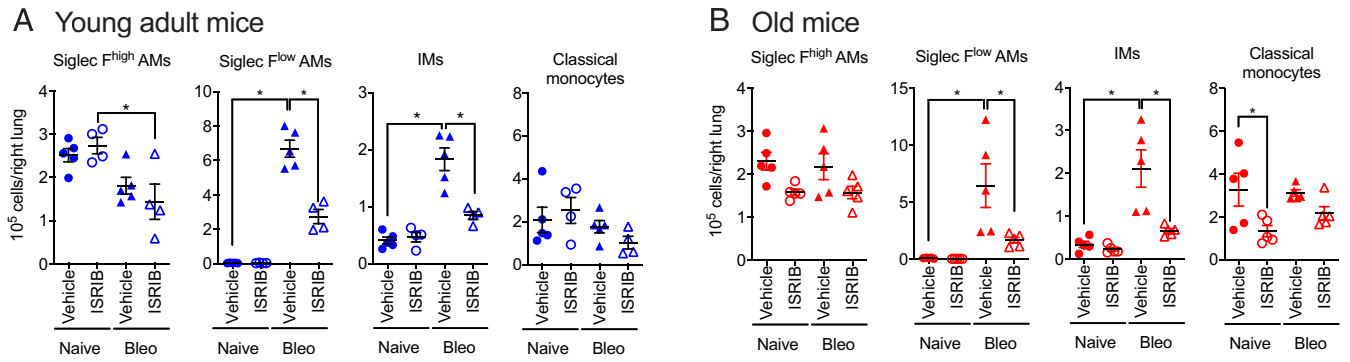

Fig. 4. ISRIB reduces the number of profibrotic monocyte-derived alveolar macrophages in lung fibrosis. Young adult (3 to 5 mo) and old (18 to 24 mo) mice were administered 0.025 unit of bleomycin (Bleo), treated with 2.5 mg/kg of ISRIB or vehicle (intraperitoneally, every day beginning at day 7), and the lungs were analyzed by flow cytometry on day 21. Alveolar macrophages (AMs) and interstitial macrophages (IMs) and classical monocytes in the lung were quantified in (*A*) young adult and (*B*) old mice. Data are shown as mean ± SEM, 4 to 5 mice per group. One-way ANOVA with Tukey test for multiple comparisons. *$P < 0.05$. Representative data from two independent experiments.

of the clusters (34). Instead, treatment with ISRIB resulted in down-regulation of genes involved in extracellular matrix remodeling, macrophage migration, and chemotaxis (Fig. 6*A*, Cluster 3) and resulted in increased expression of genes characteristic of homeostatic tissue-resident alveolar macrophages, such as lipid metabolism and phagocytosis (Fig. 6*A*, Cluster 5). We have previously shown that cell surface expression of Siglec F increases as monocyte-derived alveolar macrophages mature (22). *Siglecf*, encoding Siglec F protein, was part of the cluster 5. Supporting our hypothesis that ISRIB promotes maturation of monocyte-derived alveolar macrophages, we found that Siglec F levels were higher in GFP-positive monocyte-derived alveolar macrophages from old Cx_3cr1^{ERCre} × *zsGreen* mice treated with ISRIB compared with vehicle (Fig. 6*B*, see Fig. 5*A* for experimental design). Treatment of bleomycin-exposed young adult and old mice with ISRIB resulted in up-regulation of genes involved in biosynthetic process, proliferation, and phagocytosis (Fig. 6*A*, Cluster 1) and down-regulation of genes involved in cell cycle, antigen processing, MHC II presentation, and innate immune response (Fig. 6*A*, Cluster 2). Collectively, these results fail to show evidence for activation of the ISR in monocyte or alveolar macrophage populations in the lung during bleomycin-induced lung fibrosis but instead suggest a non-cell autonomous effect of ISRIB on alveolar macrophage maturation mediated by the lung microenvironment.

Activation of the ISR in the Alveolar Epithelium during Lung Fibrosis. Alveolar macrophages reside on the luminal side of the alveolar epithelium within the epithelial lining fluid where they are attached to epithelial cells by integrins expressed on their surface. AT2 cells secrete trophic factors including GM-CSF that are necessary for the maturation and maintenance of alveolar macrophages. Thus, the lack of transcriptomic changes in circulating monocytes and the accelerated maturation of monocyte-derived alveolar macrophages in response to ISRIB led us to hypothesize that ISRIB was promoting alveolar epithelial repair after bleomycin- or asbestos-induced injury. Consistent with this hypothesis, RNA-seq of flow-sorted AT2 cells 14 d after bleomycin-induced injury showed up-regulation of genes associated with activation of the ISR (*SI Appendix*, Fig. S7 *A–C* and Dataset S4). Additionally, we treated mice with a single dose of ISRIB or vehicle and 24 h later performed transcriptomic profiling on flow-sorted AT2 cells: 100 genes were down-regulated, and 109 genes were up-regulated (ANOVA-like test on negative binomial generalized log-linear model FDR $q < 0.05$). The up-regulated genes included genes critical to protein folding (*Hspa1a*, *Hspa1b*, *Hsph1*, *Bag3*, *Dnajb1*, and others), while down-regulated genes were enriched for biological processes related to cell death and cell differentiation (*SI Appendix*, Fig. S7*D* and Dataset S5).

ISRIB Accelerates the Differentiation of AT2 Cells into AT1 Cells. Damage to the alveolar epithelium is repaired by the proliferation of AT2 cells followed by their differentiation into AT1 cells (44). Several groups reported that an epithelial population with transcriptional features of both AT2 and AT1 cells characterized by increased expression of *KRT8* emerges during the development of pulmonary fibrosis (45–48). A homologous population of cells was identified from single-cell RNA-seq analysis of patients with pulmonary fibrosis and was also localized to areas of active fibrosis (49, 50). We observed increased expression of ATF4 target genes and *Krt8* in AT2 cells 14 d after bleomycin (*SI Appendix*, Fig. S7 *B* and *C*), a time when Strunz and colleagues observed the highest abundance of KRT8+ cells after administration of bleomycin (45). We therefore wondered whether activation of the ISR slows the transition of AT2 to AT1 cells, allowing this transitional cell population to accumulate. To test this hypothesis, we permanently labeled AT2 cells with GFP by treating young adult $Sftpc^{CreER}$ × *zsGreen* mice with tamoxifen via oral gavage 22 d before they were treated with bleomycin. We started treatment with ISRIB 7 d later followed by harvest and analysis 3 d later (day 10, Fig. 7*A*). We generated single-cell suspensions of the lung and used flow cytometry to identify GFP^+ $EPCAM^{int}MHC\ II^+$ AT2 cells and GFP^+ $EPCAM^{int}$ $PDPN^+$ AT1 cells. In ISRIB-treated compared with vehicle-treated animals, the number of GFP^+ AT1 cells was increased (Fig. 7 *B* and *C*). These results suggest that ISRIB enhances the differentiation of AT2 into AT1 cells. Consistent with this hypothesis, immunofluorescent microscopy confirmed that the number of GFP^+KRT8^+ transitional cells was reduced, and the number of GFP^+PDPN^+ AT1 cells was increased in lung sections from these mice (Fig. 7 *D* and *E*).

The administration of bleomycin has been reported to enhance the expression of CHOP in the alveolar epithelium (17). In time series single-cell transcriptomic data, Schiller and colleagues reported an increase in epithelial *Ddit3* (the gene encoding CHOP) after bleomycin administration that peaked ∼12 d after administration (45). This ISR-mediated increase in CHOP is predicted to enhance the susceptibility of the epithelium to apoptosis, and this should be relieved with ISRIB (51, 52). Accordingly, we measured apoptosis in mice treated with bleomycin followed by ISRIB treatment 6 d later and quantified the number of apoptotic cells 24 h later using dual immunohistochemistry for surfactant protein C, which marks AT2 cells, and the terminal deoxynucleotidyl transferase dUTP nick end labeling (TUNEL) assay. Treatment

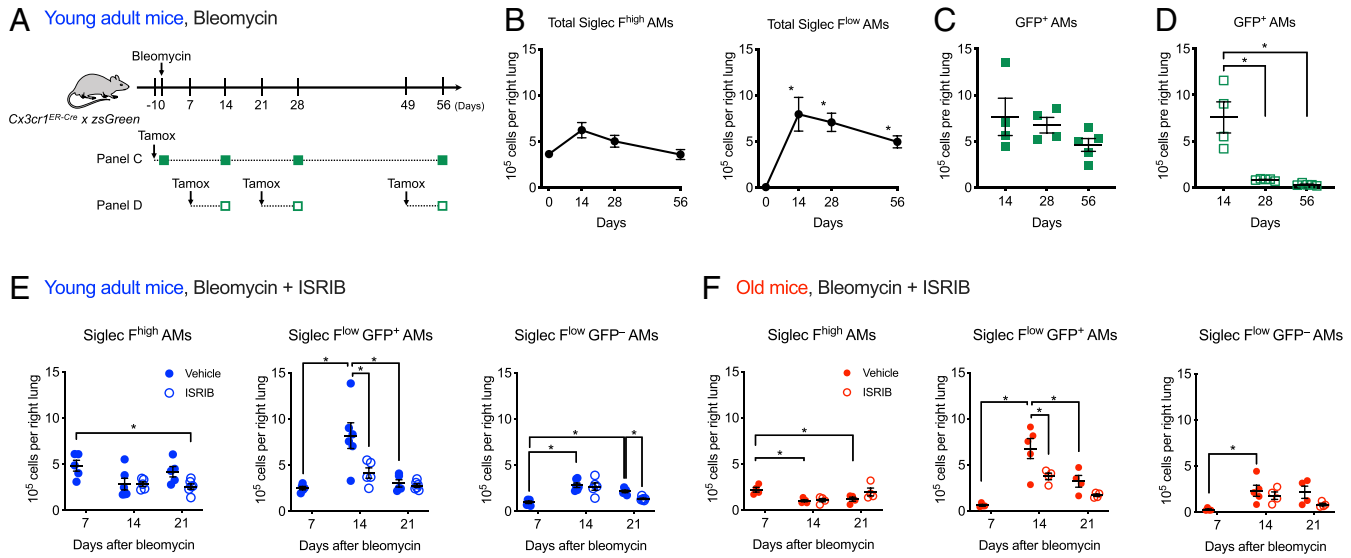

Fig. 5. ISRIB reduces recruitment of monocyte-derived alveolar macrophages during lung fibrosis. (*A*) Schematic of the genetic lineage tracing system using Cx_3cr1^{ERCre} × *zsGreen* mice in bleomycin-induced lung fibrosis. Tamoxifen treatment permanently labels circulating monocytes, which are largely replaced within 7 d (*SI Appendix*, Fig. S5*B*), but tissue-resident alveolar macrophages, which do not express *Cx3cr1*, are unlabeled. After lung injury, monocytes lineage-tagged with GFP are recruited to the lung where they differentiate into monocyte-derived alveolar macrophages. Filled squares indicate experiments where tamoxifen was given before bleomycin. Open squares indicate experiments where tamoxifen was given 7 d before harvest. (*B*) The number of total Siglec F^{high} tissue-resident alveolar macrophages (AMs) and Siglec F^{low} monocyte-derived AMs in bleomycin model. Cx_3cr1^{ERCre} × *zsGreen* mice received a single pulse of tamoxifen 1 d prior to administration of bleomycin and were analyzed at indicated time points. One-way ANOVA with Dunnett's multiple comparisons test, comparing data from each day to baseline (day 0), 3 to 5 mice per group. (*C*) The number of GFP^+ monocyte-derived alveolar macrophages remains stable over the course of bleomycin-induced fibrosis. Cx_3cr1^{ERCre} × *zsGreen* mice received a single pulse of tamoxifen 1 d prior to administration of bleomycin (intratracheal) and were analyzed at indicated timepoints. The difference between the days is not significant, one-way ANOVA with Dunnett's test for multiple comparisons. (*D*) Recruitment of monocyte-derived alveolar macrophages continues during the first 7 d of bleomycin-induced pulmonary fibrosis but ceases after 21 d. Cx_3cr1^{ERCre} × *zsGreen* mice received a pulse of tamoxifen 7 d before analysis. One-way ANOVA with Dunnett's test for multiple comparisons between day 14 and days 28 and 56. (*E* and *F*) ISRIB decreases recruitment of monocyte-derived alveolar macrophages in young adult (*E*) and old (*F*) mice. Mice received a single pulse of tamoxifen one day prior to administration of bleomycin (intrathecal) and received either with 2.5 mg/kg of ISRIB or vehicle (intraperitoneally, every day, starting at day 7) and were harvested at indicated timepoints. One-way ANOVA with Tukey test for multiple comparisons. 4 to 6 mice per group. $*P < 0.05$.

with ISRIB significantly reduced the number of TUNEL-positive AT2 cells (Fig. 7*F* and *SI Appendix*, Fig. S7*E*). This is unlikely related to the differentiation of AT2 into AT1 cells noted above, as two independent groups have shown AT2 cell differentiation into AT1 cells is achieved by asymmetric AT2 cell division (44, 53).

In young adult mice, pneumonectomy leads to the formation of new alveoli in the native lung (48). In single-cell RNA-seq data generated from young adult mice after pneumonectomy, investigators observed population of cells that were transcriptionally similar to the KRT8+ cells described above (48). If ISRIB accelerates the differentiation of AT2 to AT1 cells, we predicted it would increase the number of GFP+ AT1 cells in tamoxifen-treated $Sftpc^{CreER}$ × *zsGreen* mice after pneumonectomy. Accordingly, we treated these mice with tamoxifen and performed the pneumonectomy 14 d later. We then gave ISRIB or vehicle the next day and harvested the lungs 7 d later (Fig. 8*A*). The number of GFP^+ AT2 cells was similar in mice treated with vehicle or ISRIB (Fig. 8 *B*–*D*). The number of GFP+ AT1 cells was significantly increased in mice treated with ISRIB compared with those treated with vehicle (Fig. 8 *C* and *D*).

Discussion

Our data add to an emerging literature elucidating the multicellular nature of pulmonary fibrosis. We found that a small molecule inhibitor of the integrated stress response—ISRIB—removes a barrier to AT2 to AT1 cell differentiation induced by activation of the ISR. ISRIB accelerates the differentiation of AT2 into AT1 cells after both bleomycin and pneumonectomy and reduces alveolar epithelial apoptosis after bleomycin. Accelerated repair of the alveolar epithelium promotes the maturation of profibrotic monocyte-derived alveolar macrophages. This prevents the formation of macrophage–fibroblast circuits that drive fibroblast proliferation and matrix production (22–24, 33, 54).

ISRIB is a small molecule developed by Carmela Sidrauski and colleagues in Peter Walter's laboratory that targets the ISR (34). The ISR is activated in response to environmental or genetic stressors that threaten the proteome by activation of the kinases EIF2AK 1 to 4 in response to heme deprivation, viral infection, endoplasmic reticulum stress, or amino acid deprivation, respectively (14). These kinases all phosphorylate eIF2α, a component of eukaryotic initiation factor 2 (eIF2), which is required to initiate translation on AUG start codons as a part of eIF2-GTP-Met-tRNA ternary complex. During translation initiation, GTP is hydrolyzed to GDP, and a dedicated guanine nucleotide exchange factor for eIF2 (eIF2B) is needed to catalyze GDP to GTP exchange and reactivate eIF2 (55). ISR-induced phosphorylation of eIF2α causes it to bind tightly to eIF2B, precluding binding of the unphosphorylated protein and preventing binding to GTP (56). This inhibits bulk translation but enhances translation of proteins with inhibitory small uORFs. Important among these is ATF4, a transcription factor that drives the transcription of proteins that protect the proteome including chaperones and metabolic enzymes, among others (57). ATF4 induces the transcription of CHOP, which, upon reaching a threshold level, induces apoptosis (58). Because ISRIB enhances the guanine exchange factor activity of eIF2B in the presence of phosphorylated eIF2α, it relieves both translational inhibition and inhibits ATF4-mediated gene transcription (34, 35). Therefore, the salutary effects of ISRIB we observed on alveolar epithelial differentiation might be attributed to its effects on

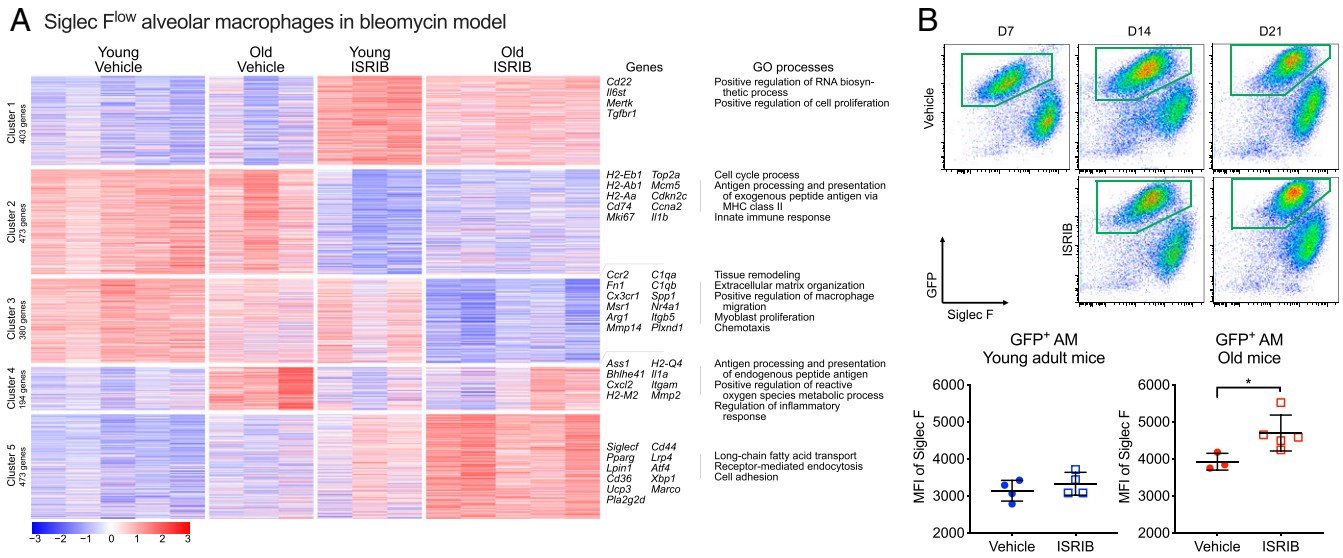

Fig. 6. Transcriptomic profiling does not reveal evidence of activation of the ISR in alveolar macrophage populations during lung fibrosis. (*A*) Transcriptomes of sorted monocyte-derived alveolar macrophages in young adult and old mice exposed to bleomycin (day 21) with and without ISRIB treatment. *k*-means clustering of all differentially expressed genes (ANOVA-like test on negative binomial generalized log-linear model, FDR *q*-value < 0.05). (*Right*) The characteristic Gene Ontology biological processes and genes associated with each cluster. (*B*) Representative flow cytometry plots gated on $CD45^{+}CD64^{+}$ macrophages in old $Cx_3cr1^{ERCre} \times zsGreen$ mice treated with tamoxifen 1 d prior to administration of bleomycin (see Fig. 5*A* for design). Median fluorescence intensity (MFI) of Siglec F levels on GFP-positive alveolar macrophages (AM) in young and old mice 21 d after bleomycin, with and without ISRIB treatment. Data are shown as mean ± SEM, 3 to 5 mice per group. Unpaired *t* test. $*P < 0.05$.

translation, the expression of ATF4-mediated genes, and prevention of CHOP-induced apoptosis (59).

In a time series analysis of single-cell RNA-seq data collected from the lungs of mice exposed to bleomycin, Strunz et al. identified a population of cells that expressed AT2 and AT1 markers in addition to increased expression of *Krt8* (45). A transcriptionally similar population of cells was observed by Kobayashi et al. during AT2 to AT1 differentiation in alveolar organoids and during bleomycin-induced fibrosis (46) and by Wu et al. after pneumonectomy (48). Kobayashi et al. suggested this transitional population represented a bottleneck in the transition from a small cuboidal AT2 cell to a large flattened AT1 cell (46). A transcriptionally similar population of cells, referred to as "aberrant basaloid cells" and marked by expression of *KRT17*, was recently identified in two single-cell RNA-seq datasets from patients with pulmonary fibrosis, and these cells were localized to areas of fibrosis in the distal lung (49, 50, 60). Transcriptional similarities between *Krt8* cells in mice and *KRT17*-expressing cells in humans include several markers typically associated with senescence (*CDKN2A*, *CDKN1A*, *SERPINE1*, *GLB1*, and *TP53*), suggesting this transitional cell population contributes to the increased markers of senescence observed in the lungs of patients with pulmonary fibrosis. Our finding that relief of the ISR is associated with a loss of this transitional cell population in mice therefore provides an alternative explanation for the increase in senescence markers reported in murine models of pulmonary fibrosis and in patients with pulmonary fibrosis (61).

Alveolar epithelial injury results in the recruitment of profibrotic monocyte-derived alveolar macrophages (22, 27, 62, 63). The precise role of these cells in fibrosis is unknown, but intriguingly, macrophages have been shown to create epithelium-like barriers in the synovium (64). We speculate that recruited monocyte-derived alveolar macrophages may function to seal the barrier induced by the loss of AT1 cells. Physical contact between monocyte-derived alveolar macrophages and matrix fibroblasts might then form a stable circuit in which the monocyte-derived alveolar macrophage is retained by fibroblast-derived M-CSF, and the monocyte-derived alveolar macrophage secretes factors promoting fibroblast proliferation and matrix production (24, 32). As the differentiating AT2 cell flattens into an AT1 cell, it disrupts interactions between monocyte-derived alveolar macrophage and matrix and simultaneously provides signals to the macrophages (e.g., GM-CSF) to mature or undergo apoptosis. Our findings support but do not prove this model. In both young and old mice, treatment with ISRIB reduced the recruitment of monocyte-derived alveolar macrophages. Furthermore, transcriptomic profiling suggested the administration of ISRIB accelerated the differentiation of monocyte-derived alveolar macrophages into mature, homeostatic tissue-resident–like alveolar macrophages. Importantly, we could not detect evidence of an ISR signal in macrophages, suggesting these effects were not cell autonomous but instead were driven by the local microenvironment.

Our data suggest an age-related decline in epithelial proteostasis resilience, as has been reported in other model organisms, might contribute to the worsened fibrosis in old compared with young adult mice (11, 12). This hypothesis would explain the link between pulmonary fibrosis risk with advanced age and with genes predicted to disrupt proteostasis in the epithelium (65). For example, a mutation in the *MUC5B* promoter associated with fibrosis results in enhanced expression of an abundant mucin secreted by lung epithelial cells (31). A mutation in *SFTPC*, the expression of which is restricted to AT2 cells, encodes a misfolded protein, and expression of this mutant in AT2 cells in mice is sufficient to induce spontaneous pulmonary fibrosis accompanied by recruitment of profibrotic monocyte-derived alveolar macrophages (26, 27, 30). Loss of function in genes associated with the Hermansky–Pudlak syndrome disrupts intracellular protein transport, and investigators have localized the effect of these mutants to the lung epithelium in mouse models (28, 29, 66). While genes involved in the maintenance of telomere length are ubiquitously expressed, loss of function mutations in these genes targeted to AT2 cells induce spontaneous or more severe fibrosis in animal models (67, 68). Finally, viruses, which challenge lung epithelial proteostasis, cause or exacerbate pulmonary fibrosis (69). Consistent with this hypothesis, genetic and pharmacologic strategies to inhibit endoplasmic reticulum stress have been reported to reduce bleomycin-induced fibrosis (17, 19, 70).

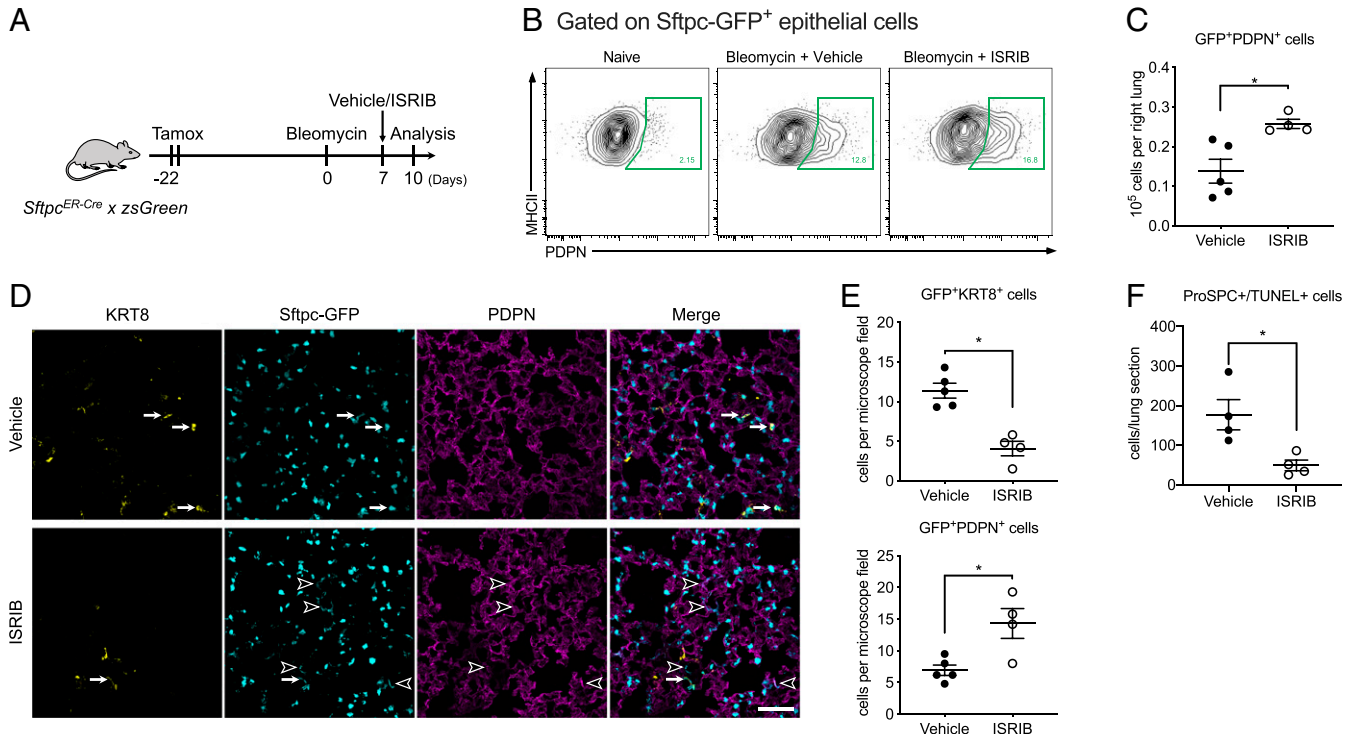

Fig. 7. ISRIB promotes alveolar epithelial differentiation after bleomycin. (*A*) Schematic of the experiment design. Young adult *Sftpc*^{ERCre} × *zsGreen* mice (3 to 5 mo) received 10 mg of tamoxifen via oral gavage on 2 sequential days 22 d prior to administration of bleomycin (0.025 units, intrathecal). Mice were treated with ISRIB 25 mg/kg intraperitoneally or vehicle 7 d after administration of bleomycin and analyzed 3 d later. (*B*) Representative flow cytometry data gated on GFP$^+$ epithelial cells. (*C*) The number of GFP$^+$PDPN$^+$ epithelial cells in vehicle- and ISRIB-treated mice was determined by flow cytometry. Unpaired *t* test, $^*P < 0.05$. (*D*) Representative lung sections stained with antibodies against KRT8 and PDPN from mice treated with bleomycin and a single dose of ISRIB or vehicle according to the timeline in *A*. The arrows indicate GFP$^+$KRT8$^+$ epithelial cells, and the arrow heads indicate GFP$^+$PDPN$^+$ AT1 cells. (Scale bar, 100 μm.) (*E*) Quantification of GFP$^+$KRT8$^+$ and GFP$^+$PDPN$^+$ epithelial cells by immunofluorescence. Average cell counts were calculated from at least five non-overlapping areas per section. Data are shown as mean ± SEM, 4 to 5 mice per group. Mann–Whitney *U* test. $^*P < 0.05$. (*F*) Quantification of double positive TUNEL and pro-SPC cells on histological sections after bleomycin. Data are shown as mean ± SEM, 4 to 5 mice per group. Mann–Whitney *U* test. $^*P < 0.05$.

We add to a growing body of literature describing the dramatic effects of ISRIB in age-related disease. A single dose of ISRIB has been shown to improve cognitive function in normal mice and in mice after traumatic brain injury (34, 36, 71), prevent neurodegeneration in murine prion disease (72), improve glucose tolerance and diabetes-induced liver injury in rats (73), prevent postnatal hearing loss in a genetic mouse model (74), reduce neuropathic pain in a murine model of diabetic neuropathy (75), alleviate dwarfism in a murine model of chondrodysplasia (76), slow the growth of metastatic prostate cancer (77), improve survival of lymphoblast cell lines from patients with vanishing white matter disease (78), and alleviate the social deficit and elevated anxiety-like behavior in a murine model of these neuropsychiatric disorders (79). Interestingly, while ISRIB improved memory in normal animals, it did not do so in two murine models of Alzheimer's disease (80, 81).

Our study has significant limitations. First, we cannot exclude an important effect of ISRIB treatment on other cells in the lung nor can we attribute the reduction in monocyte-derived alveolar macrophages to the effects of ISRIB on epithelial proteostasis. For example, endothelial cells or fibroblasts, or even cells outside the lung, for example, hematopoietic cells in the bone marrow, might contribute to the antifibrotic effects of ISRIB. Second, ISRIB both relieves translational inhibition and inhibits the expression of ATF4-mediated gene expression. Whether one or both of these is/are required for the differentiation of AT2 into AT1 cells or the amelioration of fibrosis will require additional study. Third, although mitigated by our use of flow cytometry, some of our assays relied on quantification of markers in lung tissue, which cannot be considered definitive in the absence of systematic evaluations with stereology. Lastly, our experiments were performed exclusively in male mice, and hence, we could not evaluate the importance of sex difference in aging, fibrosis, or the response to ISRIB.

In conclusion, we show that ISRIB, a small molecule that restores protein translation after activation of the ISR, can attenuate resolving fibrosis induced by bleomycin and nonresolving fibrosis induced by asbestos fibers in both young adult and old mice. ISRIB in part promotes epithelial repair after injury, secondarily accelerating the differentiation and perhaps loss of monocyte-derived alveolar macrophages. ISRIB shows promise as part of a combined strategy targeting epithelial proteostasis, pathogenic monocyte-derived alveolar macrophages, and proliferating fibroblasts to treat pulmonary fibrosis.

Materials and Methods

Methods Details. Reference *SI Appendix*, Table S1 for a detailed list of reagents.

Mice. All experimental protocols were approved by the Institutional Animal Care and Use Committee at Northwestern University. All strains including wild-type mice are bred and housed at a barrier- and specific pathogen-free facility at the Center for Comparative Medicine at Northwestern University. Young adult mice were used from 8 to 12 wk old, and over 18 mo old mice were used as old mice for all experiments. The C57BL/6J mice were obtained from Jackson Laboratories (Jax stock 000664). Old mice were obtained from the National Institute of Aging. The *Cx3cr1*^{ERCre} mice (42), *Sftpc*^{ERCre} mice (82), and *ZsGreen* (83) mice were obtained from Jackson Laboratories (Jax stocks 020940, 028054, and 007906, correspondingly). Only male mice were used in experiments.

Bleomycin- and asbestos-induced lung fibrosis and drug administration. Mice were anesthetized and intubated followed by intratracheally instillation of bleomycin (0.025 unit in 50 μL phosphate-buffered saline [PBS]) or crocidolite

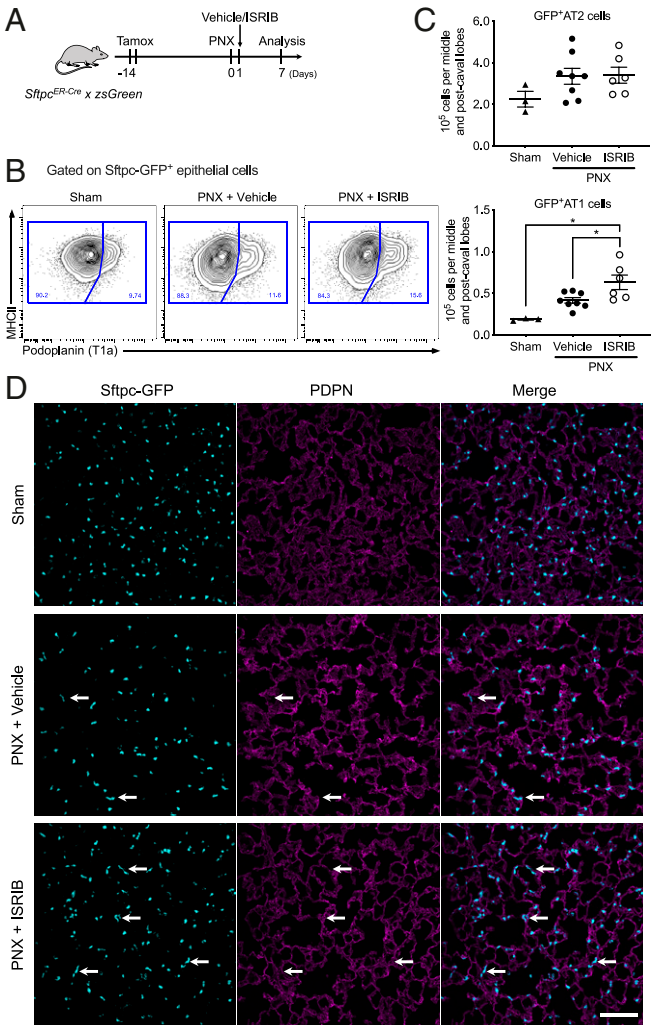

Fig. 8. ISRIB promotes alveolar epithelial differentiation after pneumonectomy. (*A*) Schematic of the experiment design. Young adult *Sftpc*^{ERCre} × *zsGreen* mice (3 to 5 mo) received 10 mg of tamoxifen via oral gavage on 2 sequential days 14 d prior to pneumonectomy (PNX). Mice were treated with ISRIB 25 mg/kg intraperitoneally or vehicle 1 d after pneumonectomy, analysis performed on day 7 after pneumonectomy on postcaval lobe. (*B*) Representative flow cytometry plots, from *Sftpc*^{ERCre} × *zsGreen* mice, gated on CD45^{-}EpCAM^{+}MHC II^{+}GFP^{+} cells. (*C*) Quantification of GFP^{+}PDPN^{-} AT cells and GFP^{+}PDPN^{+} AT1 cells in vehicle- and ISRIB-treated mice. Data are shown as mean ± SEM, 3 to 8 mice per group. One-way ANOVA with Tukey–Kramer test for multiple comparison, $*P < 0.05$. (*D*) Representative images of lung tissue (postcaval lobe) from young adult mice 7 d after pneumonectomy and a single dose of ISRIB or vehicle at day 1 postpneumonectomy. The arrows indicate GFP^{+}PDPN^{+} AT1 cells derived from GFP+ AT2 cells. (Scale bar, 100 μm.)

asbestos fibers (100 μg in 50 μL PBS) to induce lung fibrosis as previously described (22, 24). Lungs were harvested at indicated time points for flow cytometry, RNA sequencing, and histopathology. For the lineage tracing study, 100 μL 10 mg tamoxifen (Sigma, T5648) was dissolved in sterile corn oil (Sigma, C8267) and administered to the anesthetized mice by oral gavage. ISRIB (AdooQ BioScience LLC, A14302) was first reconstituted in dimethyl sulfoxide to the concentration 4 mg/mL and then further diluted using PBS to the final concentration 0.3125 mg/mL (72). ISRIB was administered via intraperitoneal injection, either via single or daily injections as indicated in the text and figure legends at the dose 2.5 mg/kg in a final volume of 200 μL. Control animals were treated using vehicle.

Pneumonectomy model. Mice were anesthetized with isoflurane and intubated with a 21G atraumatic cannula and mechanically ventilated with a mouse ventilator. We positioned the mouse in the right lateral decubitus position, made a 2 cm cut parallel to the ribs, and opened the thorax in the anterior–posterior axis. The left lung was carefully lifted, and the left main bronchus and hilar pulmonary vessels were ligated with 2-0 nylon thread. The left lung was then removed and thorax, muscle, and skin closed with 4-0 silk. For the mouse sham control, the procedure was performed without resecting the lung. Mechanical ventilation was ended after the spontaneous breathing. Postoperative pain was treated with Metacam every 12 h for 48 h or one dose of Buprenorphine sustained release subcutaneously.

Tissue preparation, flow cytometry, and sorting. Tissue preparation for flow cytometry analysis and cell sorting was performed as previously described (22, 24), with modifications. Briefly, mice were euthanized, and their lungs were perfused through the right ventricle with 10 mL Hanks' Balanced Salt Solution (HBSS). For the myeloid and lymphoid cells, the lungs were removed and infiltrated with 2 mg/mL collagenase D (Roche) and 0.2 mg/mL deoxyribonuclease I (DNase I, Roche) dissolved in HBSS with Ca^{2+} and Mg^{2+} using a syringe with a 30G needle. Lungs were chopped with scissors, and tissue was transferred into C Tubes (Miltenyi Biotech, 130-096-334) and processed in a gentleMACS Dissociator (Miltenyi Biotech) using program *m_lung_01* followed by incubation for 30 min at 37 °C with gentle agitation followed by program *m_lung_02*. The resulting single-cell suspension was filtered through a 40 μm nylon cell strainer. The cells were incubated with anti-mouse CD45 microbeads (Miltenyi Biotech, 130-052-301), and CD45^{+} cells were collected using the MultiMACS Cell24 Separator (Miltenyi Biotech) using *possel* protocol. For the epithelial cells, the lungs were removed and, using a 30G needle, infused with 1 mL dispase (Corning) with DNase I (Sigma) before incubation at room temperature with gentle agitation for 45 min followed by gentle teasing using forceps into small fragments and then incubation in digestion buffer for 15 min. The resulting suspension was passed through a 70 μm cell strainer (Falcon), washed with Dulbecco's Modified Eagle Medium (DMEM; Corning) supplemented with 5% fetal bovine serum (FBS; Corning), pelleted by centrifugation, and erythrocytes were lysed using BD Pharm Lyse (BD Biosciences). The resulting single-cell suspension was kept in DMEM/FBS and passed through a 40 μm cell strainer (Falcon) two times. Automated cell counting was performed using a Nexcelom K2 Cellometer with acridine orange and propidium iodide (AO/PI) reagent. Cells were stained with fixable viability dye eFluor 506 (eBioscience), incubated with Fc Block (BD Biosciences), and stained with a mixture of fluorochrome-conjugated antibodies as listed above. The Click-iT reaction for Alexa Fluor 647 labeling was performed using the Click-iT Plus EdU Alexa Fluor 647 Flow Cytometry Assay Kit (Thermo Fisher Scientific, C10634). Single color controls were prepared using BD CompBeads (BD Biosciences) and Arc beads (Invitrogen). Flow cytometry and cell sorting were performed at the Northwestern University Robert H. Lurie Comprehensive Cancer Center Flow Cytometry Core facility. Data were acquired on a custom BD FACSymphony instrument using BD FACSDiva software (BD Biosciences). Compensation and analysis were performed using FlowJo software (Tree Star). Each cell population was identified using sequential gating strategy (*SI Appendix*, Fig. S2). The percentage of cells in the live/singlets gate was multiplied by the number of live cells using a Cellometer K2 Image cytometer to obtain cell counts. Cell sorting was performed using a BD FACSAria III instrument using a 100 μm nozzle and 40 psi pressure.

Bulk RNA-seq. RNA was isolated using the Arcturus PicoPure RNA Isolation Kit (Thermo Fisher Scientific, catalog number KIT0204) for experiments in Figs. 6*A* and 7*C* or the AllPrep DNA/RNA Mini Kit (Qiagen, catalog number 80204) for the experiment in Fig. 6*B*. RNA quality was assessed using TapeStation 4200 (Agilent), and only samples with an RNA integrity number over seven were used for library preparation. Library construction for RNA-seq was performed using the NEBNext RNA Ultra I kit (New England Biolabs, catalog number E7530L) with the polyA messenger RNA (mRNA) isolation module (New England Biolabs, catalog number E7490S) from 30 ng (Fig. 6*B*), 3 ng (Fig. 6*A*), or 50 ng (Fig. 7*C*) of RNA. Libraries were assessed for quality (TapeStation 4200, Agilent) and then sequenced on a NextSeq 500 instrument (Illumina). FASTQ files were generated using bcl2fast (version 2.19.1) followed by quality control using FastQC, trimming using Trimmomatic (version 0.36), and mapping to the mm10 version of the mouse genome with Spliced Transcripts Alignment to a Reference aligner (STAR, version 2.6.0). Counts were generated using htseq-count (High-Throughput sequencing framework, HTSeq version 0.11.2). Differential gene expression was performed using edgeR (version 3.28.0). Raw data are available from the Gene Expression Omnibus (GEO): GSE145590 and GSE145771. The detailed R code used for analysis is available at https://github.com/NUPulmonary/2021_Watanabe.

Histopathology, immunohistochemistry, and immunofluorescence. After euthanasia and perfusion, the trachea was cannulated with a Luer syringe stub blunt needle, and mouse lungs were inflated with 4% paraformaldehyde at 15 cm H_2O column pressure. The left lung was fixed in 4% paraformaldehyde for 24 h and

dehydrated and embedded in paraffin. For histopathology, 4 μm thick sections were prepared. Hematoxylin and eosin staining and Masson's trichrome staining were performed for the analysis of fibrosis scoring. TUNEL and pro-surfactant protein C (pro-SPC) double-labeling assay was performed for the analysis of apoptotic cells with AT2 cells. Immunohistochemistry was performed at the Northwestern University Mouse Histology and Phenotyping Laboratory Core facility. Apoptotic AT2 cells (TUNEL+/pro-SPC+) were counted using Fiji (ImageJ, v.1.8.0). For immunofluorescence, mouse lung tissue was fixed in 4% paraformaldehyde for 6 h and transferred into 20% sucrose for overnight incubation. The tissue was embedded in the Tissue-Tek OCT compound (Sakura), flash frozen in liquid nitrogen, and cut on a cryostat at 14 μm thickness. Sections were air dried and stained with primary antibodies and appropriate secondary antibodies as listed above. DAPI (Invitrogen, D3571) was used for nuclear staining, and sections were mounted with ProLong Diamond Antifade Mountant (Invitrogen, P36965). Images were acquired on a Nikon A1R confocal microscope or a Nikon Ti2 wide field microscope at the Northwestern University Nikon Cell Imaging Facility and processed using Nikon Elements Software. The number of AT2 cells (Sftpc-GFP+), differentiated KRT8 cells (Sftpc-GFP+/KRT8+), and differentiated AT1 cells (Sftpc-GFP+/Pdpn+) were quantified using Fiji (ImageJ, v.1.8.0).

Fibrosis scores and lung collagen determination. Fibrosis scores were performed from Masson's trichrome-stained specimens in a blinded manner in accordance with the modified Ashcroft score for bleomycin (84) and the code set by pathology standard for asbestosis (85). Collagen levels were determined using a picrosirius red precipitation assay as described previously (22, 24). For collagen levels using second harmonic generation, the deparaffinized mouse lung tissue was imaged on a Nikon A1R MP Multiphoton Microscope at the Northwestern University Nikon Cell Imaging Facility.

Statistical analysis. Statistical tests and tools for each analysis are explicitly described with the results or detailed in figure legends.

Data Availability. Gene expression data have been deposited in the GEO database (GSE145590 and GSE145771).

ACKNOWLEDGMENTS. This work used services from Northwestern University RHLCCC Flow Cytometry Facility, Center for Advanced Microscopy, and Mouse Histology and Phenotyping Laboratory, which are supported by National Cancer Institute Cancer Center Support Grant P30 CA060553 awarded to the Robert H. Lurie Comprehensive Cancer Center. Multiphoton microscopy was performed on a Nikon A1R multiphoton microscope acquired through the support of NIH 1S10OD010398-01. This research was supported in part through the computational resources and staff contributions provided by the Genomics Computing Cluster (Genomic Nodes on Quest), which is jointly supported by the Feinberg School of Medicine, the Center for Genetic Medicine, and Feinberg's Department of Biochemistry and Molecular Genetics, the Office of the Provost, the Office for Research, and Northwestern Information Technology. S.W. is supported by MSD Life Science Foundation, Public Interest Incorporated Foundation, and the David W. Cugell and Christina Enroth-Cugell Fellowship Program at Northwestern University. P.A.R. is supported by Northwestern University's Lung Sciences Training Program 5T32HL076139-13, 1F32HL136111-01A1, and NIH K08HL146943; Parker B. Francis Fellowship; and the American Thoracic Society Foundation/Boehringer Ingelheim Pharmaceuticals Inc. Research Fellowship in IPF. R.A.G. is supported by T32AG020506-18 and F31AG071225. M.J. is supported by The Veterans Administration grant BX000201. C.J.G. is supported by NIH grants HL134800 and GM129312 and a research grant from Boehringer Ingelheim Pharmaceuticals, Inc. G.R.S.B. is supported by NIH grants ES013995, HL071643, and AG049665 and The Veterans Administration grant BX000201. A.V.M. is supported by NIH grants HL135124, HL153312, AG049665, and AI135964.

1. D. J. Lederer, F. J. Martinez, Idiopathic pulmonary fibrosis. *N. Engl. J. Med.* **378**, 1811–1823 (2018).
2. L. Richeldi, H. R. Collard, M. G. Jones, Idiopathic pulmonary fibrosis. *Lancet* **389**, 1941–1952 (2017).
3. V. J. Thannickal *et al.*, Blue journal conference. Aging and susceptibility to lung disease. *Am. J. Respir. Crit. Care Med.* **191**, 261–269 (2015).
4. G. Raghu, D. Weycker, J. Edelsberg, W. Z. Bradford, G. Oster, Incidence and prevalence of idiopathic pulmonary fibrosis. *Am. J. Respir. Crit. Care Med.* **174**, 810–816 (2006).
5. G. Raghu *et al.*, Idiopathic pulmonary fibrosis in US medicare beneficiaries aged 65 years and older: Incidence, prevalence, and survival, 2001-11. *Lancet Respir. Med.* **2**, 566–572 (2014).
6. D. C. Zank, M. Bueno, A. L. Mora, M. Rojas, Idiopathic pulmonary fibrosis: Aging, mitochondrial dysfunction, and cellular bioenergetics. *Front. Med. (Lausanne)* **5**, 10 (2018).
7. A. Pardo, M. Selman, Lung fibroblasts, aging, and idiopathic pulmonary fibrosis. *Ann. Am. Thorac. Soc.* **13**, S417–S421 (2016).
8. W. E. Balch *et al.*, Malfolded protein structure and proteostasis in lung diseases. *Am. J. Respir. Crit. Care Med.* **189**, 96–103 (2014).
9. W. E. Balch, R. I. Morimoto, A. Dillin, J. W. Kelly, Adapting proteostasis for disease intervention. *Science* **319**, 916–919 (2008).
10. J. A. Kropski, T. S. Blackwell, Progress in understanding and treating idiopathic pulmonary fibrosis. *Annu. Rev. Med.* **70**, 211–224 (2019).
11. A. Ben-Zvi, E. A. Miller, R. I. Morimoto, Collapse of proteostasis represents an early molecular event in Caenorhabditis elegans aging. *Proc. Natl. Acad. Sci. U.S.A.* **106**, 14914–14919 (2009).
12. M. Brehme *et al.*, A chaperome subnetwork safeguards proteostasis in aging and neurodegenerative disease. *Cell Rep.* **9**, 1135–1150 (2014).
13. P. M. Quirós *et al.*, Multi-omics analysis identifies ATF4 as a key regulator of the mitochondrial stress response in mammals. *J. Cell Biol.* **216**, 2027–2045 (2017).
14. K. Pakos-Zebrucka *et al.*, The integrated stress response. *EMBO Rep.* **17**, 1374–1395 (2016).
15. S. C. Wootton *et al.*, Viral infection in acute exacerbation of idiopathic pulmonary fibrosis. *Am. J. Respir. Crit. Care Med.* **183**, 1698–1702 (2011).
16. A. Burman, H. Tanjore, T. S. Blackwell, Endoplasmic reticulum stress in pulmonary fibrosis. *Matrix Biol.* **68-69**, 355–365 (2018).
17. A. Burman *et al.*, Localized hypoxia links ER stress to lung fibrosis through induction of C/EBP homologous protein. *JCI Insight* **3**, e99543 (2018).
18. E. Delbrel *et al.*, HIF-1α triggers ER stress and CHOP-mediated apoptosis in alveolar epithelial cells, a key event in pulmonary fibrosis. *Sci. Rep.* **8**, 17939 (2018).
19. H. S. Hsu *et al.*, Involvement of ER stress, PI3K/AKT activation, and lung fibroblast proliferation in bleomycin-induced pulmonary fibrosis. *Sci. Rep.* **7**, 14272 (2017).
20. B. B. Moore *et al.*, Protection from pulmonary fibrosis in the absence of CCR2 signaling. *J. Immunol.* **167**, 4368–4377 (2001).
21. M. A. Gibbons *et al.*, Ly6Chi monocytes direct alternatively activated profibrotic macrophage regulation of lung fibrosis. *Am. J. Respir. Crit. Care Med.* **184**, 569–581 (2011).
22. A. V. Misharin *et al.*, Monocyte-derived alveolar macrophages drive lung fibrosis and persist in the lung over the life span. *J. Exp. Med.* **214**, 2387–2404 (2017).
23. A. L. McCubbrey *et al.*, Deletion of c-FLIP from CD11b^{hi} macrophages prevents development of bleomycin-induced lung fibrosis. *Am. J. Respir. Cell Mol. Biol.* **58**, 66–78 (2018).
24. N. Joshi *et al.*, A spatially restricted fibrotic niche in pulmonary fibrosis is sustained by M-CSF/M-CSFR signalling in monocyte-derived alveolar macrophages. *Eur. Respir. J.* **55**, 1900646 (2020).
25. R. M. Tighe *et al.*, Recruited exudative macrophages selectively produce CXCL10 after noninfectious lung injury. *Am. J. Respir. Cell Mol. Biol.* **45**, 781–788 (2011).
26. Q. Zhong *et al.*, Role of endoplasmic reticulum stress in epithelial-mesenchymal transition of alveolar epithelial cells: Effects of misfolded surfactant protein. *Am. J. Respir. Cell Mol. Biol.* **45**, 498–509 (2011).
27. S.-I. Nureki *et al.*, Expression of mutant Sftpc in murine alveolar epithelia drives spontaneous lung fibrosis. *J. Clin. Invest.* **128**, 4008–4024 (2018).
28. L. R. Young, M. T. Borchers, H. L. Allen, R. S. Gibbons, F. X. McCormack, Lung-restricted macrophage activation in the pearl mouse model of Hermansky-Pudlak syndrome. *J. Immunol.* **176**, 4361–4368 (2006).
29. L. R. Young *et al.*, The alveolar epithelium determines susceptibility to lung fibrosis in Hermansky-Pudlak syndrome. *Am. J. Respir. Crit. Care Med.* **186**, 1014–1024 (2012).
30. A. Venosa *et al.*, Epithelial expression of an interstitial lung disease-associated mutation in surfactant protein-C modulates recruitment and activation of key myeloid cell populations in mice. *J. Immunol.* **202**, 2760–2771 (2019).
31. M. A. Seibold *et al.*, A common MUC5B promoter polymorphism and pulmonary fibrosis. *N. Engl. J. Med.* **364**, 1503–1512 (2011).
32. X. Zhou *et al.*, Circuit design features of a stable two-cell system. *Cell* **172**, 744–757.e17 (2018).
33. M. Adler *et al.*, Principles of cell circuits for tissue repair and fibrosis. *iScience* **23**, 100841 (2020).
34. C. Sidrauski *et al.*, Pharmacological brake-release of mRNA translation enhances cognitive memory. *eLife* **2**, e00498 (2013).
35. A. F. Zyryanova *et al.*, ISRIB blunts the integrated stress response by allosterically antagonising the inhibitory effect of phosphorylated eIF2 on eIF2B. *Mol. Cell* **81**, 88–103.e6 (2021).
36. A. Chou *et al.*, Inhibition of the integrated stress response reverses cognitive deficits after traumatic brain injury. *Proc. Natl. Acad. Sci. U.S.A.* **114**, E6420–E6426 (2017).
37. I. Y. Adamson, D. H. Bowden, Response of mouse lung to crocidolite asbestos. 2. Pulmonary fibrosis after long fibres. *J. Pathol.* **152**, 109–117 (1987).
38. A. V. Misharin, L. Morales-Nebreda, G. M. Mutlu, G. R. Budinger, H. Perlman, Flow cytometric analysis of macrophages and dendritic cell subsets in the mouse lung. *Am. J. Respir. Cell Mol. Biol.* **49**, 503–510 (2013).
39. A. Puchta *et al.*, TNF drives monocyte dysfunction with age and results in impaired anti-pneumococcal immunity. *PLoS Pathog.* **12**, e1005368 (2016).
40. X. Chen, O. Nadiarynkh, S. Plotnikov, P. J. Campagnola, Second harmonic generation microscopy for quantitative analysis of collagen fibrillar structure. *Nat. Protoc.* **7**, 654–669 (2012).
41. K. Krukowski *et al.*, Integrated stress response inhibitor reverses sex-dependent behavioral and cell-specific deficits after mild repetitive head trauma. *J. Neurotrauma* **37**, 1370–1380 (2020).
42. S. Yona *et al.*, Fate mapping reveals origins and dynamics of monocytes and tissue macrophages under homeostasis. *Immunity* **38**, 79–91 (2013).
43. K. M. Vattem, R. C. Wek, Reinitiation involving upstream ORFs regulates ATF4 mRNA translation in mammalian cells. *Proc. Natl. Acad. Sci. U.S.A.* **101**, 11269–11274 (2004).

44. A. N. Nabhan, D. G. Brownfield, P. B. Harbury, M. A. Krasnow, T. J. Desai, Single-cell Wnt signaling niches maintain stemness of alveolar type 2 cells. *Science* **359**, 1118–1123 (2018).
45. M. Strunz *et al*., Alveolar regeneration through a Krt8+ transitional stem cell state that persists in human lung fibrosis. *Nat. Commun.* **11**, 3559 (2020).
46. Y. Kobayashi *et al*., Persistence of a regeneration-associated, transitional alveolar epithelial cell state in pulmonary fibrosis. *Nat. Cell Biol.* **22**, 934–946 (2020).
47. P. Jiang *et al*., Ineffectual type 2-to-type 1 alveolar epithelial cell differentiation in idiopathic pulmonary fibrosis: Persistence of the $KRT8^{hi}$ transitional state. *Am. J. Respir. Crit. Care Med.* **201**, 1443–1447 (2020).
48. H. Wu *et al*., Progressive pulmonary fibrosis is caused by elevated mechanical tension on alveolar stem cells. *Cell* **180**, 107–121.e17 (2020).
49. A. C. Habermann *et al*., Single-cell RNA sequencing reveals profibrotic roles of distinct epithelial and mesenchymal lineages in pulmonary fibrosis. *Sci. Adv.* **6**, eaba1972 (2020).
50. T. S. Adams *et al*., Single-cell RNA-seq reveals ectopic and aberrant lung-resident cell populations in idiopathic pulmonary fibrosis. *Sci. Adv.* **6**, eaba1983 (2020).
51. G. R. Budinger *et al*., Proapoptotic Bid is required for pulmonary fibrosis. *Proc. Natl. Acad. Sci. U.S.A.* **103**, 4604–4609 (2006).
52. H. R. Kang, S. J. Cho, C. G. Lee, R. J. Homer, J. A. Elias, Transforming growth factor (TGF)-beta1 stimulates pulmonary fibrosis and inflammation via a Bax-dependent, bid-activated pathway that involves matrix metalloproteinase-12. *J. Biol. Chem.* **282**, 7723–7732 (2007).
53. W. J. Zacharias *et al*., Regeneration of the lung alveolus by an evolutionarily conserved epithelial progenitor. *Nature* **555**, 251–255 (2018).
54. S. H. Phan, The myofibroblast in pulmonary fibrosis. *Chest* **122**, 286S–289S (2002).
55. Y. L. Wong *et al*., eIF2B activator prevents neurological defects caused by a chronic integrated stress response. *eLife* **8**, e42940 (2019).
56. A. G. Hinnebusch, J. R. Lorsch, The mechanism of eukaryotic translation initiation: New insights and challenges. *Cold Spring Harb. Perspect. Biol.* **4**, a011544 (2012).
57. K. Ameri, A. L. Harris, Activating transcription factor 4. *Int. J. Biochem. Cell Biol.* **40**, 14–21 (2008).
58. H. Nishitoh, CHOP is a multifunctional transcription factor in the ER stress response. *J. Biochem.* **151**, 217–219 (2012).
59. H. H. Rabouw *et al*., Small molecule ISRIB suppresses the integrated stress response within a defined window of activation. *Proc. Natl. Acad. Sci. U.S.A.* **116**, 2097–2102 (2019).
60. A. Bharat *et al*., Lung transplantation for patients with severe COVID-19. *Sci. Transl. Med.* **12**, eabe4282 (2020).
61. M. J. Schafer *et al*., Cellular senescence mediates fibrotic pulmonary disease. *Nat. Commun.* **8**, 14532 (2017).
62. K. J. Mould *et al*., Cell origin dictates programming of resident versus recruited macrophages during acute lung injury. *Am. J. Respir. Cell Mol. Biol.* **57**, 294–306 (2017).
63. E. N. Atochina-Vasserman *et al*., Early alveolar epithelial dysfunction promotes lung inflammation in a mouse model of Hermansky-Pudlak syndrome. *Am. J. Respir. Crit. Care Med.* **184**, 449–458 (2011).
64. S. Culemann *et al*., Locally renewing resident synovial macrophages provide a protective barrier for the joint. *Nature* **572**, 670–675 (2019).
65. J. A. Kropski, W. E. Lawson, L. R. Young, T. S. Blackwell, Genetic studies provide clues on the pathogenesis of idiopathic pulmonary fibrosis. *Dis. Model. Mech.* **6**, 9–17 (2013).
66. L. R. Young, R. Pasula, P. M. Gulleman, G. H. Deutsch, F. X. McCormack, Susceptibility of Hermansky-Pudlak mice to bleomycin-induced type II cell apoptosis and fibrosis. *Am. J. Respir. Cell Mol. Biol.* **37**, 67–74 (2007).
67. J. M. Povedano, P. Martinez, J. M. Flores, F. Mulero, M. A. Blasco, Mice with pulmonary fibrosis driven by telomere dysfunction. *Cell Rep.* **12**, 286–299 (2015).
68. R. P. Naikawadi *et al*., Telomere dysfunction in alveolar epithelial cells causes lung remodeling and fibrosis. *JCI Insight* **1**, e86704 (2016).
69. T. R. McMillan *et al*., Exacerbation of established pulmonary fibrosis in a murine model by gammaherpesvirus. *Am. J. Respir. Crit. Care Med.* **177**, 771–780 (2008).
70. E. A. Ayaub *et al*., GRP78 and CHOP modulate macrophage apoptosis and the development of bleomycin-induced pulmonary fibrosis. *J. Pathol.* **239**, 411–425 (2016).
71. Y. Sekine *et al*., Stress responses. Mutations in a translation initiation factor identify the target of a memory-enhancing compound. *Science* **348**, 1027–1030 (2015).
72. M. Halliday *et al*., Partial restoration of protein synthesis rates by the small molecule ISRIB prevents neurodegeneration without pancreatic toxicity. *Cell Death Dis.* **6**, e1672 (2015).
73. V. K. Pandey, A. Mathur, M. F. Khan, P. Kakkar, Activation of PERK-eIF2α-ATF4 pathway contributes to diabetic hepatotoxicity: Attenuation of ER stress by Morin. *Cell. Signal.* **59**, 41–52 (2019).
74. J. Li *et al*., Deletion of Tmtc4 activates the unfolded protein response and causes postnatal hearing loss. *J. Clin. Invest.* **128**, 5150–5162 (2018).
75. P. Barragán-Iglesias *et al*., Activation of the integrated stress response in nociceptors drives methylglyoxal-induced pain. *Pain* **160**, 160–171 (2019).
76. C. Wang *et al*., Inhibiting the integrated stress response pathway prevents aberrant chondrocyte differentiation thereby alleviating chondrodysplasia. *eLife* **7**, e37673 (2018).
77. H. G. Nguyen *et al*., Development of a stress response therapy targeting aggressive prostate cancer. *Sci. Transl. Med.* **10**, eaar2036 (2018).
78. Y. L. Wong *et al*., The small molecule ISRIB rescues the stability and activity of Vanishing White Matter Disease eIF2B mutant complexes. *eLife* **7**, e32733 (2018).
79. Z. D. Kabir *et al*., Rescue of impaired sociability and anxiety-like behavior in adult cacna1c-deficient mice by pharmacologically targeting eIF2α. *Mol. Psychiatry* **22**, 1096–1109 (2017).
80. D. I. Briggs *et al*., Role of endoplasmic reticulum stress in learning and memory impairment and Alzheimer's disease-like neuropathology in the PS19 and APP^{Swe} mouse models of tauopathy and amyloidosis. *eNeuro* **4**, ENEURO.0025-17.2017 (2017).
81. E. C. Johnson, J. Kang, A small molecule targeting protein translation does not rescue spatial learning and memory deficits in the hAPP-J20 mouse model of Alzheimer's disease. *PeerJ* **4**, e2565 (2016).
82. J. R. Rock *et al*., Multiple stromal populations contribute to pulmonary fibrosis without evidence for epithelial to mesenchymal transition. *Proc. Natl. Acad. Sci. U.S.A.* **108**, E1475–E1483 (2011).
83. L. Madisen *et al*., A robust and high-throughput Cre reporting and characterization system for the whole mouse brain. *Nat. Neurosci.* **13**, 133–140 (2010).
84. R. H. Hubner *et al*., Standardized quantification of pulmonary fibrosis in histological samples. *Biotechniques* **44**, 507–517 (2008).
85. D. W. Kamp *et al*., Phytic acid, an iron chelator, attenuates pulmonary inflammation and fibrosis in rats after intratracheal instillation of asbestos. *Toxicol. Pathol.* **23**, 689–695 (1995).